Journal of Physics D: Applied Physics

PAPER

Characteristics of a propagating, self-pulsing, constricted ‘γ-mode-like’ discharge

To cite this article: Daniel Schröder *et al* 2015 *J. Phys. D: Appl. Phys.* **48** 055206

J. Phys. D: Appl. Phys. **48** (2015) 055206 (11pp) doi:10.1088/0022-3727/48/5/055206

Characteristics of a propagating, self-pulsing, constricted 'γ-mode-like' discharge

Daniel Schröder, Sebastian Burhenn, Teresa de los Arcos and Volker Schulz-von der Gathen

Institute for Experimental Physics II, Ruhr- Universität Bochum, Universitätsstraße 150, 44801 Bochum, Germany

E-mail: daniel.schroeder@rub.de

Received 11 November 2014, revised 16 December 2014
Accepted for publication 17 December 2014
Published 19 January 2015

Abstract

Investigations on the self-pulsing operation regime of a modified micro-scaled atmospheric pressure plasma jet (μ-APPJ) are presented. Using a wedge-shaped electrode configuration, a self-pulsing behavior of the device is achieved, which is characterized by the repetitive ignition of a constricted 'γ-mode-like' discharge at the gas inlet, which propagates with the gas flow towards the nozzle, where it extinguishes. The 'γ-mode-like' feature coexists with the homogeneous alpha-glow. Synchronized voltage/current and optical emission measurements are presented in order to correlate the evolution of electrical quantities such as voltage, current, dissipated power and phase with changes in the discharge structure. First insights are gained into the underlying discharge dynamics responsible for a stable self-sustainment, propagation and extinction of the constricted discharge. The results indicate that processes induced by helium metastables play a major role. Maximal electron densities on the order of $n_e = 3.2 \cdot 10^{12}$ cm^{-3} and dissipated power of 18.9 W are achieved in this novel operation regime.

Keywords: microplasma, atmospheric pressure, self-pulsing, alpha glow, gamma-mode, instability, discharge modes

(Some figures may appear in colour only in the online journal)

1. Introduction

Atmospheric pressure plasmas with micro- to millimeter dimensions stand out due to their non-equilibrium electron-driven chemistry at low gas temperatures. This unique characteristic makes so-called 'microplasmas' attractive for many applications, in particular in the manifold and strong interdisciplinary field of plasma medicine [1–4]. Microplasmas are capable of producing a great variety of chemical reactive species and photons needed in the treatment of heat-sensitive biological materials like cells, skin tissue, and microorganisms [5]. Examples of possible applications are their ability to support wound healing processes or the sterilization of biologically contaminated materials [6–8].

Microplasma jets are a promising group of these devices, which allow a localized treatment with species that, after being produced in the active plasma region, are steered with the afterglow towards the substrates being treated. However, while the number of jet devices and their applications is increasing continuously, the basic, underlying physics are still not completely understood [9, 10]. In particular, capacitively coupled (micro-) discharges with radio-frequency excitation and operated at high pressures are susceptible to instabilities. Two such examples are the 'thermal' instability and the 'α–γ transition' instability, whose appearance limits the stable and reproducible long-term operation/application of these devices [4, 11]. Both result in the formation of a localized 'arc' discharge characterized by high temperatures and bright plasma luminosity, which can lead to the destruction of the device due to the high thermal load [12–15]. Hence, the safe application of these discharges to heat-sensitive materials is not guaranteed.

One well-investigated device is the micro-scaled Atmospheric Pressure Plasma Jet (μ-APPJ) based on a jet design by Selwyn and co-workers [16, 17]. At room temperature and with an atmospheric pressure helium gas flow at 13.56 MHz excitation, the device forms a homogeneous, stable glow discharge. By adding small amounts of molecular oxygen or nitrogen as precursors, high densities of reactive oxygen and nitrogen species (RONS) as well as high energetic UV-radiation are produced, which all are accounted to be responsible for the bactericidal activity of the plasma discharge [18, 19]. It has been shown that the composition of the reactive species produced in the μ-APPJ can be tailored for a specific application by varying the applied sender power: e.g. atomic oxygen density grows with increasing power, whereas the ozone density decreases [20, 21]. However, at high applied sender powers the μ-APPJ undergoes a transition to the arc-like destructive operation regime.

In order to overcome the self-destruction at high powers, we modified the μ-APPJ by using a wedge electrode configuration instead of a coplanar one. Like the coplanar device, above a distinct voltage threshold, a constricted high-luminosity discharge ignites (α–γ transition). However, in the modified device, the wedge configuration forces this feature to move along the electrodes, thus resulting in a self-pulsing behavior. This prevents the discharge from developing into a stationary arc damaging the device. This particular operation is defined as self-pulsing operation regime. The cycle starts with the ignition at the narrowest electrode gap and ends when the constricted discharge extinguishes at the nozzle. This cycle of the 'self-pulsing μ-APPJ' (SP-μ-APPJ) repeats naturally with up to kHz frequency and will be referred to in the following text as a 'pulse'. It was demonstrated for the SP-μ-APPJ that plasma chemistry could be tuned selectively for the production of atomic oxygen and ozone [22].

Different kinds of self-pulsing operations have been also observed in other plasma sources. For example, the so-called 'gliding arc', in atmospheric pressure discharges [23], or in micro-hollow cathode discharges at medium pressure regime [24].

However, the SP-μ-APPJ is an ideal model to investigate the processes determining the transition between the discharge modes in atmospheric RF discharges due to its optical accessibility, its stable repetitive manner and its long time thermal stability.

In this work, we concentrate on the two discharges modes characterizing the self-pulsing operation regime, the homogeneous α-mode glow and a 'γ-mode-like' constricted discharge. The characteristics of the constricted discharge i.e. its ignition and the formation of a stable 'γ-mode-like' are studied in detail. Furthermore, the change in discharge structure during propagation and extinction is investigated. Therefore, electrical measurements and phase-resolved optical imaging synchronized to the self-pulsing are applied.

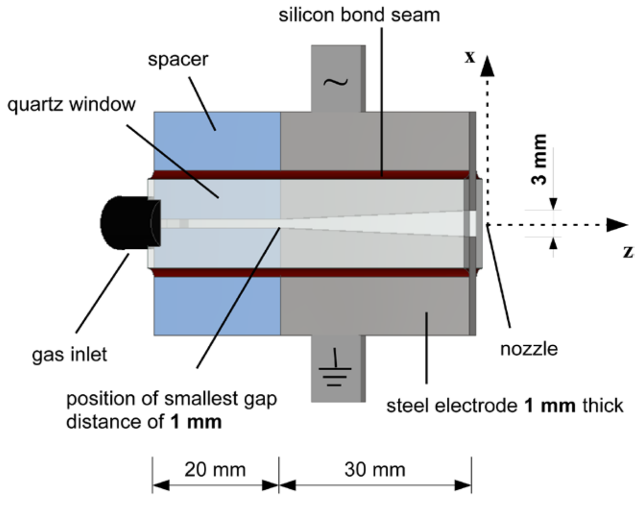

Figure 1. The SP-μ-APPJ wedged electrode configuration. The origin of the coordinate system applied here is on the discharge axis at the nozzle as indicated by the black dashed arrows.

2. Experimental setup and diagnostics

2.1. The self-pulsing micro-scaled atmospheric pressure plasma jet (SP-μ-APPJ)

The 'self-pulsing' μ-APPJ is a modification of the well-studied original coplanar μ-APPJ described in detail elsewhere [16]. Its centerpiece consists of two stainless steel electrodes arranged in a wedge-shaped configuration (see figure 1). The electrodes are one millimeter thick and 30 mm long, forming a diverting discharge gap increasing linearly from one millimeter to three millimeters at the nozzle. The smallest gap distance of one millimeter is identical to the one of the coplanar design. The direction along the electrodes is defined as z-axis with the smallest gap distance at $z = -30$ mm and $z = 0$ mm at the nozzle. The inter-electrode direction will be denoted as x-axis throughout the text with $x = 0$ mm at the center of the discharge gap.

In order to enclose the discharge volume, the electrodes are covered by quartz windows from both sides (Corning 7980). The use of quartz allows spectroscopic analysis down to the UV-range and it resists high thermal loads. The stack, consisting of windows and electrodes, is glued air-tight by a high temperature-stable silicone (UHU-500653: $T_{\max} = 260$ °C). The silicone prevents air intrusion into the discharge volume. Even at high temperatures and long operation, the silicone's flexibility prevents a possible break of the windows due to the different thermal expansion coefficients of steel and quartz. The bond seam is situated at the outer edge of the quartz windows to circumvent a possible interaction between plasma and silicone.

A sinusoidal, rf-voltage signal at 13.56 MHz frequency is applied to one of the electrodes via an impedance matching network; the other electrode is grounded (see figure 2). Between the electrode configuration and the gas inlet (6 mm tubing) a coplanar spacer region is inserted made of 20 mm long quartz panes with one millimeter separation. The additional length allows optical access to the electrode region without limitation by vignetting. Thus, even the plasma volume at the smallest gap distance can be investigated optically with a maximum

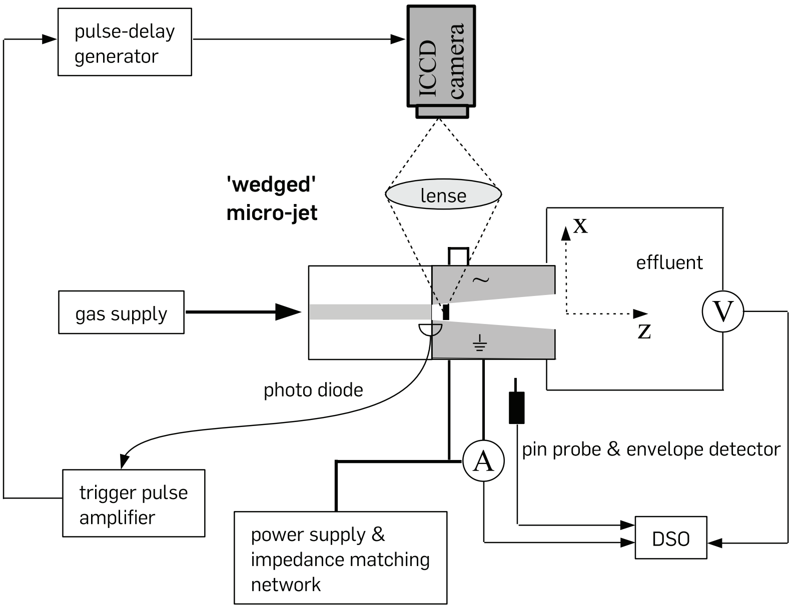

Figure 2. Experimental setup for synchronized electrical characterization and phase-resolved optical emission imaging. Synchronization of electronic measurements to the self-pulsing is realized by using a pin probe and an envelope detector to generate a kHz trigger signal for the oscilloscope. Optical imaging is synchronized to the ignition of the constricted discharge at the position of smallest gap distance ($z = -30$ mm) via a trigger signal generated by a photodiode and amplified.

solid angle. The feed gas flow of pure helium is steered by a mass flow controller and kept constant at 2 slm for all measurements shown in this publication.

2.2. Electrical diagnostics setup

In order to characterize the electronic behavior of the jet during self-pulsing, fast probes capable of resolving the 13.56 MHz excitation (Tektronix: P5100A, 500 MHz, and CT-2, 200 MHz) are used. The voltage probe is directly attached to the electrodes, whereas the current probe (current transistor) is placed around the ground wire of the respective electrode (see figure 2). Measurements in the self-pulsing operation regime are synchronized to the voltage drop associated with the ignition of the constricted discharge (see section 3.1) as the start of a 'pulse'. The signal is picked up capacitively by a pin probe and filtered by an envelope detector consisting of a diode and a low-pass filter, yielding only the kHz-components, before it is used to trigger the oscilloscope. The signal waveforms are fed to a digital storage oscilloscope (DSO) with 2 GHz bandwidth and a digitizing rate of 10 GS s^{-1} (LeCroy,WavePro 735zi). The storage depth allows to save, in self-pulsing operation, the complete current and voltage waveforms of a 833 μs pulse-cycle and still phase-resolve each rf-period of about 74 ns within the pulse with a time resolution of 0.1 ns.

The phase-shift between current and voltage signals is calculated using a home-made routine that determines the positive zero-crossings in every rf-cycle. For this, a repetitive linear interpolation within decreasing intervals close to the zero crossing (nested intervals) is used. Then, the average of all values is taken as the particular zero-crossing. Using this data processing, phase-shifts between voltage and current can be determined with an accuracy of ± 0.2° within each period. To account for the influence of the probes and the different cable lengths on the phase-shift between the two signals, the plasma-off-case at sender powers below ignition is measured and the resulting phase defined as −90° i.e. the device is regarded as an ideal capacitor. By this procedure, changes in discharge impedance and power are determined during a pulse. For the discharge impedance, RF-excited capacitively coupled discharges are described in electrotechnical terms as a series connection of two capacitors, an inductance and a resistor. The capacitors represent the sheaths, whereas the resistor and the inductance represent the different properties of the plasma bulk (electron–neutral collission, electron inertia), respectively [25].

For both operations regimes (cw and self-pulsing), the dissipated power within one rf-cycle is calculated from the obtained waveforms $U(t)$ and $I(t)$ by

$$<P_{\rm diss}> = \frac{1}{T}\int_0^T U(t)\cdot I(t)\,{\rm d}t \tag{1}$$

with $T = 1/f$. To overcome the electronic noise of the 8-bit analog to digital converter of the DSO, a floating average was applied on the two original signals. The error of these power determinations is large for small power values, but decreases with increasing powers. For the power range covered in this contribution (see figure 4(*a*)), the values have an accuracy of 0.03 W.

For comparison, the dissipated power in cw operation has been additionally determined using the calculated phase-shift by

$$<P_{\rm diss}> = \frac{1}{2}\hat{U}(t)\cdot\hat{I}(t)\,\cos(\varphi), \tag{2}$$

where $\hat{U}(t)$, $\hat{I}(t)$ denote the signal amplitudes, respectively. This is possible for the cw mode showing a pure sinusoidal signal waveform, but not for the self-pulsing operation as shown in figures 3(*a*) and (*b*).

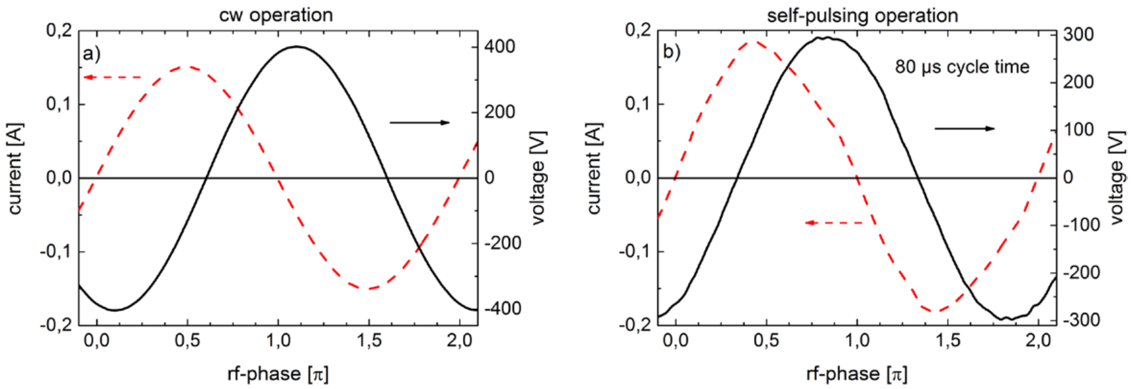

Figure 3. (*a*) Voltage (black, solid line) and current (red, dashed line) waveforms in the cw- operation mode. Both show a sinusoidal behavior. (*b*) Voltage (black, solid line) and current (red, dashed line) waveforms in the self-pulsing operation mode. Both waveforms strongly deviate from a pure sinusoidal curve.

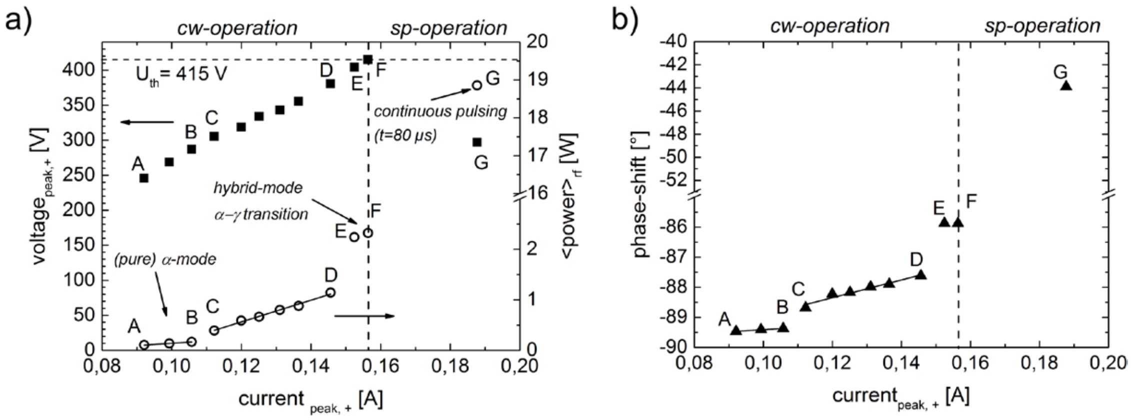

Figure 4. (*a*) I–V curve (full squares) and I–P curve (open circles) for the SP-μ-APPJ in helium with 2 slm gas flow. Depending on the current (applied sender power is steadily increased), the device can operate in different operation regimes (in either a cw-operation or a self-pulsing operation regime). (*b*) shows the respective evolution in phase-shift (full triangles).

2.3. Optical diagnostics setup

Phase-resolved imaging of the complete discharge volume with high spatial and temporal resolution is realized by the experimental setup illustrated in figure 2. The application of a gateable ICCD camera (Andor: iStar DH320) allows to display the evolution of the structure of the discharge, while it ignites, propagates along the electrodes and finally extinguishes. The synchronization of the camera to the self-pulsing is realized by a photodiode, placed at the position of smallest gap distance. The signal generated when the constricted discharge passes is amplified, delayed by a delay generator and fed as trigger signal to the ICCD camera. The spatial resolution defined by the optical system and the dimension of the camera pixel is about 40 μm. A detailed description of the setup, including a discussion on adequate synchronization, can be found in a previous publication [22].

3. Results and discussion

The most straightforward (spatially integrating) method to evaluate the operation of the microjet device is to measure electrical properties like current, voltage and phase between them. As a secondary, but convenient parameter, the actual dissipated power can be derived.

3.1. Different operation regimes and their discharge modes

Figure 4(*a*) exemplarily illustrates the current–voltage (I–V) (full squares) and the current–power (I–P) (open circles) dependencies of the SP-μ-APPJ. Here, the positive peak values for current $I_{\text{peak},+}$ and voltage $U_{\text{peak},+}$ of the measured waveforms are displayed. Figure 4(*b*) depicts the respective evolution of the phase-shift (full triangles). Depending on the current, the device can be operated in two different operation regimes, i.e. the cw-operation regime (low current, low applied sender power) and the self-pulsing operation regime (high current, high applied sender power). They should not be confused with the various discharge modes occurring within the operation regimes as described below.

3.1.1. cw-operation regime.

(Pure) α-mode. At sender powers yielding gap voltages below $U_{\text{th,peak},+} = 415$ V (horizontal dashed line in figure 4(*a*)), the wedge-shaped device operates in the homogeneous cw-regime, like the original coplanar device [16]. At ignition (A), i.e. at a positive voltage amplitude of $U_{\text{peak},+} = 245$ V and a phase-shift between current and voltage of $\phi_{UI} = -89.5°$, the plasma only expands to about one-fourth of the discharge channel in the region close to the smallest gap distance ($z = -30$ mm). The dissipated power

is about $P_{\text{diss},p}$ = 0.10 W. The plasma emission consists of an homogeneous glow with bright structures placed several hundred micrometers in front of each electrode surface This is characteristic for a bulk-ionization determined 'α-mode' glow discharge [26]. With increased sender power, the plasma expands laterally along the electrodes. Voltage, dissipated power and phase-shift grow linearly in this region until point B is reached, where the plasma extends to about half of the discharge channel.

Transition: B–C. Increasing further the sender power to point C, the voltage continues to rise to about $U_{\text{peak},+}$ = 305 V. However, the dissipated power undergoes an abrupt jump from 0.16 W to 0.39 W. The jump in power is correlated to a phase jump from −89.4° to −88.7°, which indicates that the discharge becomes less capacitive. This might be attributed to the onset of additional ionization processes such as secondary electron emission at the surface, or surface-near processes in the sheaths, like Penning ionization of nitrogen impurities and pooling reaction among helium metastables [27]. As the plasma volume does not grow during this transition, it seems to be more favorable for the discharge to initiate additional processes to sustain itself than to increase the discharge volume by breakdown at a larger discharge gap.

Region C–D. In the region from point C to D, the measured gap voltage, dissipated power and phase show a linear behavior with growing sender power, until at point D a voltage of $U_{\text{peak},+}$ = 380.5 V and a dissipated power of $P_{\text{diss},p}$ = 1.14 W at a phase ϕ_{UI} = − 87.6° are reached. This linear dependence, normally typical for abnormal glow discharges at atmospheric pressure [28], is in this case mainly due to the expansion of the discharge volume in a linear increasing electrode configuration. The plasma volume fills now almost the complete channel volume.

Transition to hybrid-mode. By further increasing the sender power, the discharge undergoes a second transition, indicated by a steep rise in dissipated power and a decrease in phase. At point E, the power rises to about $P_{\text{diss},p}$ = 2.24 W at a phase angle of ϕ_{UI} = − 85.9°. Anew, the capacitative contribution to the discharge impedance decreases. In this regime, the discharge is sustained by ionization by the formerly mentioned additional mechanisms in an amount comparable to the volume-based ionization. In literature, it is addressed to as 'hybrid-mode' or 'α–γ transition' regime [21, 27, 29]. By increasing the sender power to point F, the discharge volume grows to fill the electrode configuration completely.

3.1.2. The self-pulsing operation regime. Beyond point F ($U_{\text{th,peak},+}$ = 415 V), the device enters the so-called 'self-pulsing' operation regime, characterized by a decrease in voltage, a clear increase in phase shift and power, and ignition of a 'constricted discharge' feature of high luminosity at z = − 30 mm. It subsequently propagates towards the nozzle (z = 0 mm) until it extinguishes at some lateral position z along the electrode configuration. The particular position is determined by the voltage needed to sustain the discharge at wider discharge gap distances. During its complete lifespan, equivalent to 'self-pulsing-cycle' or 'pulse', this feature co-exists with a homogeneous glow that fills the complete volume (see figure 6). As voltages are lower than in the cw-operation, light intensity of the 'background' glow is decreased compared to the glow in the cw-operation regime, but still fills the complete discharge channel.

At voltages just above the threshold F (not shown in figure 4), constricted discharges appear randomly, propagating only to about half of electrode length (z = − 15 mm). By steadily increasing the sender power, they merge into a continuous sequence of individual constricted discharges self-pulsing at a stable frequency (see section 3.2 and [22]). The sender power is further increased until the constricted discharge can be sustained at the maximum discharge gap of 3 mm. This specific operational condition, i.e. stable continuously self-pulsing along the complete electrode length, has been chosen for the investigations described in the following (point G), with a minimal voltage of 297 $V_{p,+}$, a maximal power surge of 18.8 W and a phase-shift of −44.5°, all measured at t = 80 μs after the ignition (see figure 5).

Figure 5 illustrates the evolution of voltage, discharge current, phase-shift and dissipated power, during one self-pulsing cycle of about 833 μs duration at 1.2 kHz. Figure 5(*a*) shows the positive envelopes of the actual voltage (black curve) and current signal (red curve) consisting of the positive maxima of each rf-period, respectively. Figure 5(*b*) displays the shift in phase between current and voltage (red curve) as well as the corresponding behavior of the calculated rf-averaged dissipated power (black curve).

At t = 0 μs the constricted discharge ignites, characterized by a steep decrease in voltage. Within the first 80 μs ('ignition phase'), it drops about 30% from about 410 $V_{p,+}$ to the minimal value of about 300 $V_{p,+}$, whereas the discharge current rises to its maximum value of 0.19 A. Simultaneously phase and input power increase to their maximum values (ϕ_{UI} = − 44.5°, $P_{\text{diss},p}$ = 18.80 W) indicating a significant resistive contribution. At a cycle time of about t = 1 μs all four quantities show an abrupt change in behavior. The voltage stops falling and shows a local maximum before decreasing to its minimum value. In contrast, the discharge current simultaneously undergoes a fast drop. Dissipated power and phase show a similar, but less distinctive behavior as the current. This striking behavior of the electric quantities during the ignition phase will be investigated in detail in the next section (see section 3.3).

The following time interval from 80 μs to about 750 μs cycle time will be called 'propagation phase', as here the constricted discharge mostly propagates throughout the discharge channel (see section 3.3.2). It is characterized on the one hand by linearly increasing voltage (corresponding to the increase of the discharge gap while propagating) and on the other hand linearly decreasing current, power and phase.

The final time interval of the self-pulsing cycle is referred to as 'extinction phase', where the electric quantities deviate from the linear behaviour shown in the previous phase. While keeping their trend, the slope of voltage increase and phase decrease change by about a factor of five. At the end of that phase, the quantities have reached their starting values of the ignition phase at t = 0 μs.

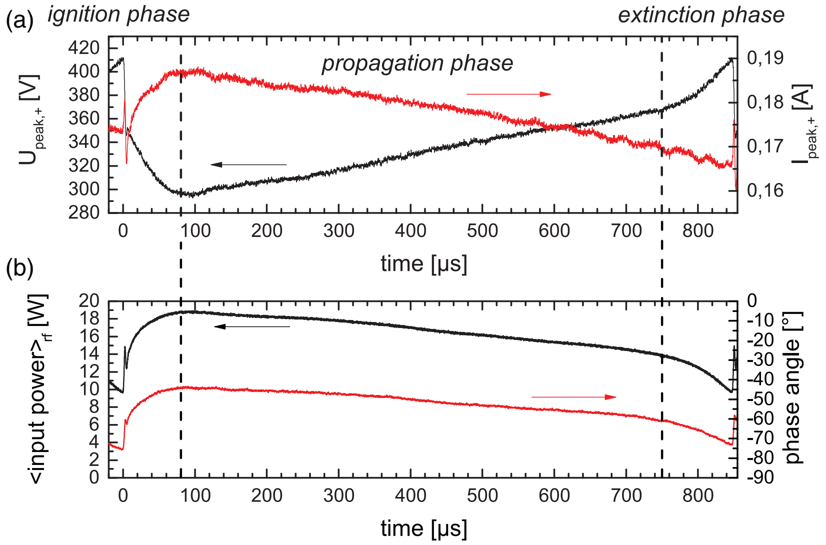

Figure 5. (*a*) Voltage (black) and current (red) evolution during one self-pulsing cycle at 1.2 kHz frequency, 21 W sender power and 2 slm feed gas flow. (*b*) Corresponding power (black) and phase (red) evolution. Due to the characteristic evolution of the electric quantities, the self-pulsing cycle can be divided into the three phases (vertical dashed lines): *ignition*, *propagation* and *extinction*.

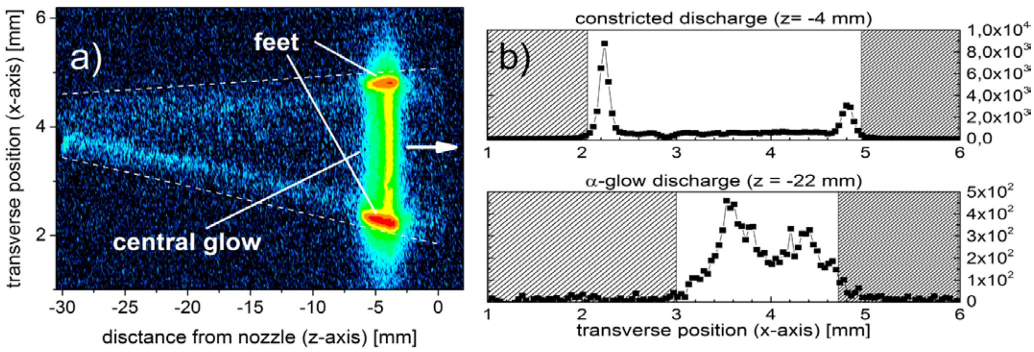

Figure 6. (*a*) Phase resolved ICCD camera image (gate width = 5 ns) of plasma emission of the jet in self-pulsing operation (720 μs cycle-time) at 21 W sender power, 2 slm helium gas flow and 1.2 kHz pulsing frequency. The scale of the false color image is logarithmic. Two different discharge modes can be identified by their characteristic emission. At $z = -4$ mm, the 'constricted' discharge overlays the homogeneous alpha-glow. (*b*) Corresponding intensity distributions between the electrodes for the constricted discharge (top) and the coexisting homogeneous α-mode glow at $z = -22$ mm (bottom). The glow emission is measured by blocking the intense emission of the constricted discharge, using 60 s integration time and a 5 ns long gatewidth.

The minimal dissipated power within the complete cycle is about 10 W, five times higher than the maximal power surge in cw-operation. The highest phase angle between voltage and current is up to −75.6° compared to −85.9°. Consequently, the device behaves substantially more resistive than in cw-operation.

3.2. Coexistence of α-glow and constricted 'γ-mode- like' discharge

Electrical measurements are global and thus cannot discriminate between discharge features such as constricted and homogeneous glows. A correlation to those can be achieved by applying Phase Resolved Imaging (PRI). Figure 6(*a*) shows a false color image of the spectrally integrated plasma emission of the complete discharge volume in the self-pulsing operation at $t = 720$ μs cycle-time. The measurement has been carried out with an exposure time of 2 s and a gate width of 5 ns, yielding an integration of plasma emission over 2400 self-pulsing cycles at the frequency of 1.2 kHz. As the intensities of the different emission features differ by two orders of magnitude, logarithmic scaling is used. The dashed white lines indicate the edges of the electrodes and the white arrow the direction of the gas flow.

The co-existence of two different discharge modes can be clearly seen in the figure. A few hundred micrometers distant from the electrode edges, symmetric broad emission structures are visible, which extend along the complete length of the electrodes. These are characteristic for the so-called homogeneous 'α-mode' glow in capacitive coupled rf-discharges, where the plasma is mainly sustained by volume ionization [26]. The typical emission of the positive column in the center of the two structures cannot be displayed here, since it is too weak referring to capture parameters of the camera used here. At $z = -4$ mm, the emission of a very bright, constricted discharge can be observed. It consists of two broad structures ('feet') of several millimeters in width at a close distance to the electrode surfaces. These feet are interconnected by a less

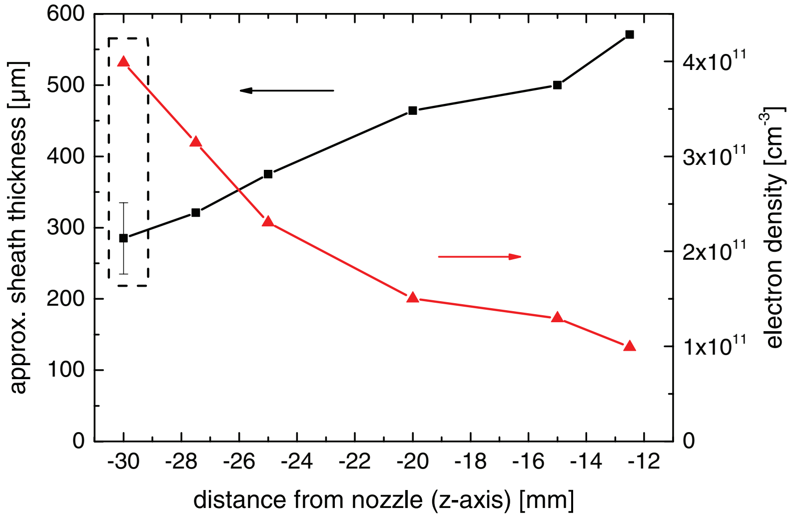

Figure 7. Sheath thickness and electron density as a function of lateral position z at operation parameters at the threshold of operation mode transition (point F in figure 4). Thicknesses have been estimated via the distance of sheath emission maxima and electrode edge. Electron densities are calculated assuming a matrix sheath model [30]. The values at 1 mm gap distance ($z = -30$ mm) are compared to a 1D hybrid model for the coplanar device (black dashed square) [21, 31].

intense central, columnar structure ('central glow') of about 0.7 mm in width (FWHM), which is slightly bent in the gas flow direction.

Figure 6(*b*) shows the corresponding vertical intensity distributions of the co-existing discharges. At the bottom the α-glow emission at $z = -22$ mm, where the dark spaces between each emission structure and the respective electrode edge are attributed to the positive space charge sheaths typical of the α-mode. The glow emission is measured by blocking the intense emission of the constricted discharge, using 60 s integration time and a 5 ns long gatewidth. Hence, the absolute intensities of both discharges cannot be related to each other in this figure.

In the top figure (constricted discharge), the emission profile of the constricted discharge resembles those of rf-excited discharges at moderate and atmospheric pressure, when operated in the so-called 'γ-mode' shown by Raizer *et al* and Yang *et al*, respectively [28, 25]. This particular discharge mode is characterized by (I) intense sheath emission, (II) a high increase in power density due to a decrease in phase, (III) a drop in voltage compared to the α-glow mode and (IV) secondary electron emission from the electrode surface sustaining this discharge [13, 15, 25, 28].

Since our device shows the same characteristics in the self-pulsing operation (see figures 4–6), it is reasonable to assume that our constricted discharge can be identified as the known 'γ-mode' discharge of rf-excited capacitively-coupled plasmas.

The two main characteristics of a γ-mode discharge are on the one hand, the transition from an α-glow induced by the α-sheath breakdown and on the other hand, the sustainment of the discharge by secondary electron emission at the electrode surfaces (γ-coefficient). The first means that the voltage across the α-glow sheath in the cw-operation (point E, F in figure 4) exceeds the breakdown voltage of a gas gap of the same size [12]. To estimate a value for the sheath thickness s we take the distance between the sheath emission maxima and the electrode edges for the α-glow in the 'hybrid-mode' i.e. on the verge of transition to the self-pulsing regime and ignition of a constricted discharge [21, 27]. This is correlated very crudely in the so-called ion sheath model i.e. ions at rest in the sheath to the averaged sheath ion density by

$$s \approx \sqrt{\frac{2\epsilon_0 V_0}{q_e n_s}} \qquad (3)$$

[30]. Here, ϵ_0 is the dielectric constant, V_0 the sheath voltage (assumed to be the rms value of the measured peak voltage), q_e the elementary charge and n_s the respective sheath ion density. Figure 7 shows the measured sheath-thickness and the calculated bulk electron density as a function of lateral position (z-axis).

The sheath thickness (black squares) increases with growing gap distance, whereas the electron density (red circles) decreases. The values of $n_e = 4.0 \cdot 10^{11}$ cm^{-3} and $s = 285$ μm at the position $z = -30$ mm (1 mm wide electrode gap) are in good agreement with the values resulting from a 1D hybrid-model for the co-planar μ-APPJ in this particular hybrid mode developed by Waskoenig for pure Helium without admixtures [21, 31]. For an assumed power density of 3 W cm^{-2} in the simulation, compared to the measured power density of 7.4 W cm^{-2}, an rf-averaged sheath thickness of 250 μm (FWHM) and an electron density of $n_e = 1.2 \cdot 10^{11}$ is calculated. The difference by roughly a factor of two in power density might be explained by the double plasma volume (6 mm^3) of the wedge-shaped electrode configuration compared to the coplanar one (3 mm^3). The model predicts the transition into the 'γ-mode' if the applied power is increased.

Since, concerning the SP-μ-APPJ, electron density is maximal and sheath thickness is minimal at the position of smallest gap distance ($z = -30$ mm), the ignition of the constricted discharge is possibly achieved by sheath breakdown mechanisms at this position. This agrees with the PRI measurements that show how the 'γ-mode' discharge always ignites at just this position within each self-pulsing cycle (see figure 8(*c*), (i)).

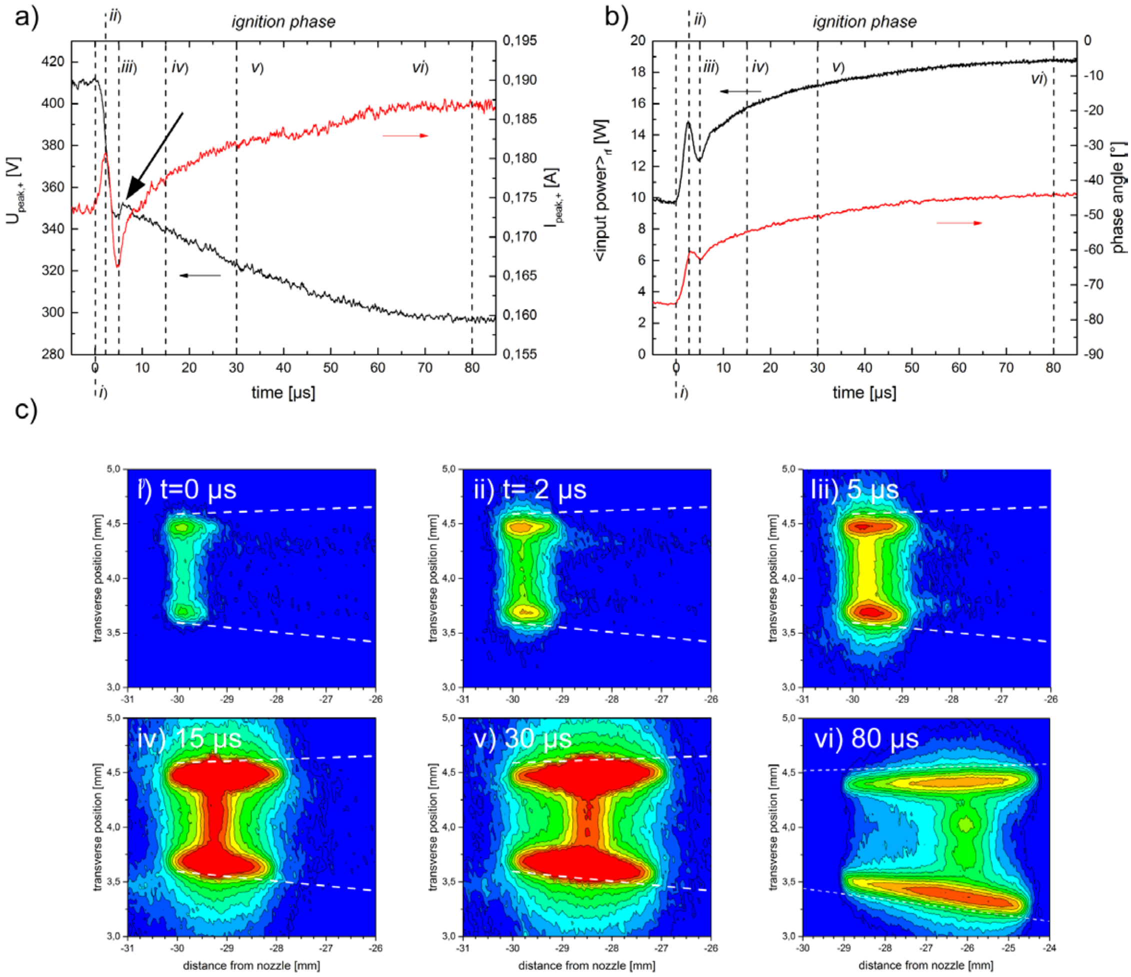

Figure 8. Correlation of the evolution of voltage (black), current (red) (subfigure *a*), phase (red) and dissipated power (black) (subfigure *b*) with the evolution of the constricted discharge shape as observed by plasma emission (subfigure *c*). Images of the constricted discharge have been taken for times marked in the figure by the black, vertical dashed lines. For the ICCD images (*c*) the same logarithmic scaling has been used for all sub-figures (i)–(vi). The dashed white lines indicate the electrode surfaces.

The repetitive nature of our discharge makes it possible to provide novel experimental evidence on the sheath-breakdown by investigating the ignition processes using phase-resolved imaging (PRI) on a nanosecond timescale synchronized to the ignition.

Concerning the sustainment of a 'γ-mode' discharge at atmospheric pressure it is has been stated in literature that Penning ionization of nitrogen by helium metastables and pooling reactions of the latter are key mechanisms to sustain the discharges in the α- as well as in the 'γ-mode' in contrast to secondary electron emission from the electrodes like in the low pressure case [29]. Therefore, the term 'γ-mode-like discharge' might be more reasonable [27, 31].

In order to tackle this issue, we have investigated the time- and space resolved behavior of helium metastables in the self-pulsing operation. The results of this investigation can be found in a recent publication of the authors [33].

Addressing the coexistence of both types of discharges (α and γ), an explanation for atmospheric pressure plasmas has been given by Moon *et al* based on the work of Raizer *et al* for the medium pressure regime [15, 25]. This phenomenon occurs if the minimum voltage during the self-pulsing cycle (here about 300 V, see figure 5) is sufficiently high to maintain an α-glow in the discharge gap (see figure 4). This is the case as the minimum voltage to sustain a pure α-glow is as low as 245 V.

3.3. Constricted γ-mode-like discharge

3.3.1. Ignition and formation of a stable discharge. A comparison of high temporal resolution of electrical and optical measurements allow a detailed insight into the specific discharge processes throughout a self-pulsing cycle. Figure 8 shows the evolution of the electric quantities (peak voltage, peak current, phase, input power) for the first 80 μs within a cycle (figures 8(*a*) and (*b*)) and the corresponding ICCD images of the spectral integrated plasma emission of the constricted discharge for selected cycle times (figure 8(*c*), logarithmic scaling). The dashed white lines in figure 8(*c*) indicate the edges of the first four millimeters of the electrode configuration. The optical measurements have been carried out with a gate width of 5 ns and an exposure time of 2 s. The emission from the coexisting α-glow is not visible in the images due to the great difference in light intensity between the two discharge modes (see figure 6(*b*)).

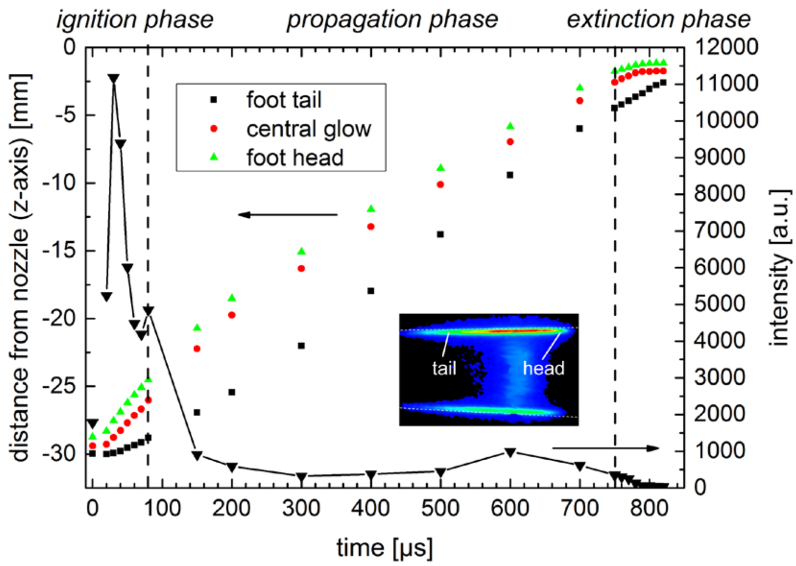

Figure 9. Left ordinate: Location of the constricted discharge within the self-pulsing cycle. Right ordinate: Emission intensity of the central glow within the self-pulsing cycle. The sub-image illustrates exemplarily the shape of the constricted discharges with foot head and foot tail labeled.

As discussed previously, at the time of ignition ($t = 0$ μs), a narrow discharge (full width half maximum (FWHM) of the upper foot of about 500 μm) forms at $z = -30$ mm due to the α-sheath breakdown accompanied by a fast drop in voltage and rise in current, phase and dissipated power. Two microseconds later ($t = 2$ μs), the width of the discharge increases to 700 μm and the emission of the feet structures and the central glow have gained intensity (image ii)). At this moment, the voltage is still dropping, whereas current, phase and dissipated power reverse their trends. At $t = 5$ μs, the width increase continues ($FWHM \simeq 900$ μm), the voltage has decreased to its local minima of $U_{\mathrm{th,peak,+}} = 346$ V and current, phase and power have undergone an abrupt drop to their local minima of 0.17 A, −62.7° and 12.3 W, respectively.

This behavior can be explained by the appearance of an ionization wave, formed as a result of the sheath breakdown, which travels through the gap between the electrodes [25]. The maxima at $t = 2$ μs of current, phase and power, occur when the wave has crossed the complete discharge gap. After the ionization wave has passed, excited states and an amount of seed metastables states, have been created as indicated by the growth in width and intensity of plasma emission at $t = 5$ μs (see figure 9). Hence, a drop of current, power and an increase in phase towards a more capacitative behavior is observed, since the energy loss of the electrons, due to the excitation processes, might diminish the electron amplification.

As the sheath-breakdown and electron dynamics occur on nanosecond timescale of the corresponding rf-excitation frequency and the ionization wave has expired, discharge processes, induced by long-living species with lifetimes of microseconds must be responsible for this distinct ‘slow’ evolution within the first five microseconds. Reasonable candidates for such processes are the above mentioned Penning ionization and the pooling reactions, induced by the ‘seed’ metastables, produced in the course of the ionization wave, which have lifetimes of microseconds at atmospheric pressure [32]. Therefore, it can be assumed that helium metastables determine the discharge dynamics here and in the complete self-pulsing cycle.

In order to further sustain the discharge and to increase the discharge current again, the voltage grows now to its distinctive local maximum of about 350 V (arrow in figure 8(a)). This is a typical behavior for a discharge in the abnormal glow regime [26]. The effective electron temperature rises, that initiates self-amplifying ionisation processes like Penning Ionization and metastable pooling reactions, leading to an increase in plasma emission intensity to its maximum (at about $t = 30$ μs), and growth of the different structures of the constricted discharge. During this phase, the width of the ‘feet’ in the images indicates that the constricted discharge is not fully established, since it is smaller than the width in the propagation phase by a factor of two ($t > 80$ μs, [22]). This evolution can be seen in image (iv) and (v) of figure 8(c) for $t = 15$ μs and $t = 30$ μs, respectively, yielding a continuous growth of current accompanied with the decrease in voltage and phase, until about a time of $t = 80$ μs.

At this point, the formation process of a stable discharge is finished and the discharge takes its final shape (see image vi). This consists of long and thin sheaths (feet) close to the electrodes and a less intense central glow (comp. figure 6(a)). The ‘γ-mode-like’ constricted discharge is now self-sustaining, with a minimal voltage of 297.0 V and maximal current and power of 0.188 A, 18.9 W (see point G in figure 4). Applying the same estimation procedure to determine the bulk electron density, a value of $n_e = 3.2 \cdot 10^{12}$ cm^{-3} is obtained, which is one order of magnitude higher than in the cw-operation regime. Sheath-thicknesses are in the order of 100 μm.

3.3.2. Propagation. Figure 9 shows on the one hand (right ordinate) the evolution of the emission intensity of the constricted discharge within the self-pulsing cycle. For the sake of clarity, only the behavior of the central glow is shown. (The emission of the two feet structures shows the same trend). The displayed intensity values have been determined in the center of the glow along the central axis of the discharge channel. Here, the emission maximum during the ignition phase at about t = 30 μs can be seen clearly, indicating the increasing contribution of sufficiently energetic electrons (see section 3.3.1).

In order to get an idea of mechanisms responsible for the propagation and the necessary sustainment of the constricted discharge, phase-resolved imaging has been applied. This is illustrated in figure 9 by the temporal evolution of the constricted discharge shape, where the time in the self-pulsing cycle starting at the ignition (t = 0 μs) at the gas inlet (z = − 30 mm) correlates with the spatial position (left ordinate) of the particular discharge structures within the discharge volume (see section 3.3.1). For analysis of the shape, characteristic points of the discharge structure are chosen i.e. the foot tail (black squares), the foot head (green triangles), and central glow (red circles). The position of feet head and tail are determined from the ICCD images by taking the first pixel position with a measurably intensity above noise level. For the sake of clarity, both are labelled in the sub-image of figure 9. The vertical distance between the points at one particular time indicates the lateral width of a feet structure.

For the first 5 μs after ignition at z = − 30 mm, the sheath is symmetrically positioned around the discharge core (see figure 8(c)) and no propagation is observed. Then the foot head accompanied by the central glow starts to propagate towards the nozzle. The foot tail stays located at the gas inlet for about 30 μs, after which it copropagates along the electrodes. During the propagation, the distance between foot head and tail firstly expands from about 2.5 to a maximum of 6 mm after about one third of the electrode length (z ∼ − 20 mm, t ∼ 200 μs). During this time, the central glow moves forward from a relatively central position at 45% of the foot length to a position 25% of the lateral foot width behind the leading head. Beyond this point, the lateral feet widths seem to continuously reduce to about 3 mm at the nozzle. It has to be noted that due to the reduction in intensity the determination of the exact feet widths is more difficult in this time period. For most of the distance, the relative position of the central glow stays constantly at a value of about 30% . At about 750 μs (extinction phase), in the vicinity of the nozzle, firstly the feet heads and then the central glow stop propagating while the feet tails keep propagating for about 50 μs, before stopping as well.

Apart from the above described behavior, the shape of the constricted discharge does not change during the complete 'propagation phase'(t = 80–750 μs). It resembles the emission structure at a cycle time of t = 80 μs shown in figure 8(c). The propagation velocity, indicated by the changing slopes of the curves, was explained by the authors in a previous publication in the image of a neutral gas volume traveling with the laminar gas flow at a given temperature in a diverting discharge channel [22]. This is in contrast to a propagation dominated by drifts of charged particles or thermal processes like buoyancy as for example in gliding arc discharges [23]. Therefore, it stands to reason, that the neutral species propagating with the gas flow and sustaining the discharge, are the helium metastables. During the ignition process, a cloud of 'seed' metastables is produced, that is then pushed forward by the gas. The metastables can then initiate further ionization, which is necessary to sustain the discharge at a wider gap distance. This is supported by the behavior of the self-pulsing frequency under a variation of the feed gas flow. It grows linearly from 900 Hz to 1500 Hz with increasing Helium flows.

3.3.3. Extinction. At about t = 750 μs (extinction phase), the foot head of the constricted discharge arrives at the nozzle of the device (see figure 9). The voltage and the absolute value of the phase increase abruptly, whereas the dissipated power decreases (see figure 5). The discharge current, on the one hand, keeps the previous linearly decreasing trend. As the metastables are pushed by the gas flow out of the discharge channel, the production of charge carriers fades. This cannot be compensated by the production of new ones, since the electric field is too weak at the large gap distance at this position (Δx = 3 mm), even when increasing the voltage drop to the maximal possible value. This results in a more capacitive behavior of the discharge and reduces the dissipated power. A further loss channel for charge carriers is quenching by intruding molecular nitrogen from the ambient air impeding the sustainment of the discharge [32]. Thus at t = 833 μs, the voltage drop at this set of operation parameters exceeds the necessary voltage to reignite at the favorable condition of the lateral position of smallest gap distance (Δx = 1 mm, z = − 30 mm). The discharge extinguishes at the nozzle at t = 833 μs and a new self-pulsing cycle is started.

4. Conclusion and outlook

The self-pulsing operation regime of a wedge-shaped micro-scaled atmospheric pressure plasma jet has been investigated (SP-μ-APPJ). At constant operation parameters, it is characterized by the coexistence of a homogeneous 'α-glow' and a constricted 'γ-mode-like' discharge. The constricted discharge ignites repetitively at the gas inlet at a frequency of 1.2 kHz, and propagates with the gas flow through the discharge channel towards the nozzle, where it extinguishes. During the ignition period, which last about 80 μs, the constricted discharge builds up to a stable and self-sustained one. First, an ionization wave, induced by the breakdown of the alpha-glow sheath (α–γ transition or instability), produces a pool of 'seed'-metastables, which then initiate the onset of charge multiplication processes. Meanwhile the discharge undergoes an 'abnormal' regime, indicated by high emission intensity, before it reaches its stable state with minimum voltage and maximal dissipated power. Electron densities are one order of magnitude higher than in the equivalent coplanar device.

Furthermore the change of discharge shape during propagation and extinction has been investigated in order to gain information about possible species involved. The results suggest that helium metastables induced processes such as Penning ionization and pooling reactions play an important role in the sustainment and the propagation dynamics of the constricted discharge. Helium metastable densities are measured time- and space-resolved, synchronized to the self-pulsing by tunable diode laser absorption spectroscopy (TDLAS) [33].

The stable repetitive manner of this device allows the experimental investigation (proof) of ignition processes like α-sheath breakdown. This will be carried out by the authors using phase-resolved optical emission spectroscopy on the ns-timescale synchronized to the ignition.

Acknowledgments

The authors gratefully acknowledge the support by the DFG in the frame of the Research Unit FOR1123 'Physics of Microplasmas' within the Research Department 'Plasma with Complex Interactions' of the Ruhr-Universität Bochum. For valuable discussion and experimental support the authors like to thank K Niemi, T Gans and D O' Connell of the University of York.

References

[1] Becker K, Koutsospyros A, Yin S-M, Christodoulatos C, Abramzon N, Joaquin J C and Brelles-Mariño G 2005 *Plasma Phys. Control. Fusion* **47** B513–23
[2] Iza F, Kim G J, Lee S M, Lee J K, Walsh J L, Zhang Y T and Kong M G 2008 *Plasma Process. Polym.* **5** 322–44
[3] Kong M G, Kroesen G, Morfill G, Nosenko T, Shimizu T, van Dijk J and Zimmermann J L 2009 *New J. Phys.* **11** 115012
[4] Fridman A 2008 *Plasma Chemistry* (Cambridge: Cambridge University)
[5] Graves D B 2012 *J. Phys. D: Appl. Phys.* **45** 263001
[6] Sladek R E J, Stoffels E, Walraven R, Tielbeek P J A and Koolhoven R A 2004 *IEEE Trans. Plasma Sci.* **32** 1540–3
[7] Stoffels E, Flikweert A J, Stoffels W W and Kroesen G M W 2002 *Plasma Sources Sci. Technol.* **11** 383–8
[8] Becker K H, Schoenbach K H and Eden J G 2006 *J. Phys. D: Appl. Phys.* **39** R55–70
[9] Laroussi M and Akan T 2007 *Plasma Process. Polym.* **4** 777–88
[10] Laimer J and Störi H 2007 *Plasma Process. Polym.* **4** 266–74
[11] Chirokov A V and Fridman A 2005 Stability of atmospheric pressure glow discharges *PhD Thesis* Drexel University
[12] Shi J J, Deng X T, Hall R, Punnett J D and Kong M G 2003 *J. Appl. Phys.* **94** 6303
[13] Shi J J and Kong M G 2005 *J. Appl. Phys.* **97** 023306
[14] Lisovskiy V, Booth J-P, Landry K, Douai D, Cassagne V and Yegorenkov V 2006 *Phys. Plasmas* **13** 103505
[15] Moon S Y, Rhee J K, Kim D B and Choe W 2006 *Phys. Plasmas* **13** 033502
[16] Schulz-von der Gathen V, Schaper L, Knake N, Reuter S, Niemi K, Gans T and Winter J 2008 *J. Phys. D: Appl. Phys.* **41** 194004
[17] Schütze A, Jeong J Y, Babayan S E, Park J, Selwyn G S and Hicks R F 1998 *IEEE Trans. Plasma Sci.* **26** 1685–94
[18] Moravej M, Yang X, Barankin M, Penelon J, Babayan S E and Hicks R F 2006 *Plasma Sources Sci. Technol.* **15** 204–10
[19] Sousa J S, Bauville G, Lacour B, Puech V, Touzeau M and Ravanat J-L 2010 *Appl. Phys. Lett.* **97** 141502
[20] Ellerweg D, Benedikt J, von Keudell A, Knake N and Schulz-von der Gathen V 2010 *New J. Phys.* **12** 013021
[21] Waskoenig J, Niemi K, Knake N, Graham L M, Reuter S, Schulz-von der Gathen V and Gans T 2010 *Plasma Sources Sci. Technol.* **19** 045018
[22] Schröder D, Burhenn S and Kirchheim D 2013 *J. Phys. D: Appl. Phys.* **46** 464003
[23] Alexander F, Nester S, Kennedy L A, Saveliev A and Mutaf-Yardimci O 1998 *Prog. Energy Combust. Sci.* **25** 211–31
[24] Rousseau A and Aubert X 2006 *J. Phys. D: Appl. Phys.* **39** 1619–22
[25] Raizer Y 1995 *Radio-Frequency Capacitive Discharges* (Boca Raton, FL: CRC)
[26] Raizer Y 1991 *Gas Discharge Physics* (Berlin: Springer)
[27] Niemi K, Waskoenig J, Sadeghi N, Gans T and O'Connell D 2011 *Plasma Sources Sci. Technol.* **20** 055005
[28] Yang X, Moravej M, Nowling G R, Babayan S E, Panelon J, Chang J P and Hicks R F 2005 *Plasma Sources Sci. Technol.* **14** 314–20
[29] Liu D W, Iza F and Kong M G 2008 *Appl. Phys. Lett.* **93** 261503
[30] Lieberman M A and Allan J. Lichtenberg 2005 *Principles of Plasma Discharges, Materials Processing* 2nd edn (Hoboken, NJ: Wiley-Interscience)
[31] Waskoenig J 2010 Numerical simulation of the electron dynamics in single and dual radio-frequency driven atmospheric pressure plasmas and associated plasma chemistry in electro-negative He- O2 mixtures *PhD Thesis* Queen's University Belfast
[32] Niermann B 2011 *J. Phys. D: Appl. Phys.* **44** 325201
[33] Spiekermeier S, Schröder D, der Gathen Schulz-von V, Böke M and Winter J, 2015 *J. Phys. D: Appl. Phys.* **48** 035203